# Synthesis, Structural And Magnetic Properties Of $Srfe_{12}O_{19}$ Hexaferrites

**S. J. MARGARETTE, A. VENKATESWARA RAO, RAGHAVENDRA VEMURI, N. MURALI, Y. RAMAKRISHNA, V. VEERAIAH, M. INDIRA DEVI**

**Abstract:** In this study, $SrFe_{12}O_{19}$ hexaferrites is synthesized by citrate sol-gel auto-combustion route. The standard analytical techniques such as X-ray Diffraction analysis (XRD), Field Effect Scanning Electron Microscopy (FE-SEM), Energy-Dispersive Spectroscopy (EDS), Fourier Transformer Infrared (FT-IR) Spectroscopy, Raman spectroscopy and magnetic studies (VSM) are applied to study the characteristics of the sample prepared. The X-ray diffraction patterns are used to analyse the structural properties of the sample. The information about the particle formation and size are obtained using scanning electron microscope (SEM). An energy-dispersive x-ray analysis tool (EDX) provides the elemental composition of the nano-particle. The Fourier transform infrared (FT-IR) spectra revealed about the functional group bonds between metal and oxygen (M–O). The vibrating sample magnetometer (VSM) technique, which is recorded at room temperature, revealed the magnetic properties of the sample with the hysteresis loops showing its magnetic behaviour.

**Keywords:** M-type hexaferrites, FE-SEM, Raman, VSM.

## 1. INTRODUCTION

In the year 1950, M-type strontium hexa-ferrite ($SrFe_{12}O_{19}$) is discovered by Philips' laboratories [1]. The M-phase ferrites (Pb, Sr, Ba)$Fe_{12}O_{19}$ have magneto-plumbite structure which are commonly called as hexagonal ferrites. As compared to the other M-phase ferrites, strontium ferrite ($SrFe_{12}O_{19}$), is an important member of hexa-ferrites series. The saturation magnetization is higher, Curie temperature is high, the magneto-crystalline anisotropy is large, conductive losses are low with high permeability. These ferrites also have excellent chemical stability and corrosion resistivity with high coercivity [2-4]. All these properties of strontium ferrites made it the popular option for its usage in industrial applications like electromagnetic wave absorber ferrox dures, perpendicular magnetic recording media, magnetic recording media, microwave devices, magnetic fluids, magnetic coatings, magnetic catalysts and so on [5-14], optoelectronic materials [15-30] and energy materials [30-50] . Basing on their chemical and crystalline structures, these ferrites are divided into five categories. The five types are (a) M-type ($SrFe_{12}O_{19}$), (b) W-type ($SrM_2Fe_{16}O_{27}$), (c) Y-type ($SrM_2Fe_{12}O_{22}$), (d) X-type ($Sr_2M_2Fe_{28}O_{46}$) and (e) Z-type ($Sr_2M_2$-$Fe_{24}O_{41}$). There is a combination of two structural blocks, which are stacked along the c-axis in the crystal structure of magneto-plumbite unit cell of the M-type hexagonal ferrite.


- S. J. MARGARETTE, Department of Physics, Andhra University, Visakhapatnam, Andhra Pradesh, India
- VENKATESWARA RAO, Department of Physics, Koneru Lakshmaiah Education Foundation, Vaddeswaram, AP, India
- RAGHAVENDRA VEMURI, Department of Physics, Aditya College of Engineering and Technology, Surampalem, India
- N. MURALI, Department of Engineering Physics, Andhra University College of Engineering (A), Andhra University, E-mail: muraliphdau@gmail.com
- Y. RAMAKRISHNA, Department of Engineering Physics, Andhra University College of Engineering (A), Andhra University
- V. VEERAIAH, Department of Physics, Andhra University, Visakhapatnam, Andhra Pradesh, India
- M. INDIRA DEVI, Department of Physics, Andhra University, Visakhapatnam, Andhra Pradesh, India


The crystal structure consists of 10 hexagonally close-packed oxygen layers in the pattern of RSR*S*. Here S block stands for spinel structure and R block stands for hexagonal structure. When R block is rotated by 180° with respect to c-axis having equivalent atomic arrangements, we get R* blocks. Likewise when S block is rotated, we get S* blocks. [15, 16]. At the $Fe^{3+}$ or $Sr^{2+}$ sites or both, the substitution of cations from metal ions to rare earth elements is done. This resulted in the improvement in the various properties of the hexa-ferrites. The preparation of solids is carried out by single source precursor since it provides excellent control over the stoichiometry. The other preparation methods are also adopted to synthesize strontium hexa-ferrite like hydrothermal method, sono-chemical method, reverse micelle technique, micro-emulsion, combustion routes, co-precipitation and sol-gel. As compared to all the other methods, sol–gel is advantageous since it maintains excellent homogeneity of the product, better compositional control and processing at lower temperatures [17-25]. Here, we report that the structural, spectroscopic and magnetic study of $SrFe_{12}O_{19}$ ferrites, which are synthesized by sol-gel auto-combustion method. The crystal structure with respect to the vibrational and magnetic properties is investigated along with the explanation of the atomic arrangement in $SrFe_{12}O_{19}$ hexaferrites.

## 2. PREPARATION AND EXPERIMENTAL TECHNIQUES

$SrFe_{12}O_{19}$ hexaferrites are prepared by sol-gel auto-combustion method using $Sr(NO_3)_2$, $Fe(NO_3)_3.9H_2O$, and $C_6H_8O_7.H_2O$ as precursors. All the reagents are weighed in stoichiometric portions. Strontium and cerium nitrate are diluted into methanol, and ferric nitrate into 10 ml of methanol. The solutions of all the nitrate salts are combined together in a 250 ml beaker, with the aqueous solution of citric acid that acts as the chelating agent. The beaker is placed on a hot plate with continuous stirring, maintaining at 80°C. The solution changed into a viscous solution and finally to a thick viscous gel after evaporation. This constant stirring continued for nearly 12 to 18 h. The gel is converted to ash coloured powder on the removal of all water molecules from the mixture. This was followed by preheating at 900 °C for 2 h to remove the volatile

compounds and further heat treatment is carried out at 1200 °C at a rate of 5 °C per minute for 2 h to enhance the crystalline property. Rigaku Cu-Kα diffractometer is used for powder X-ray diffraction (XRD) data of the sample with diffraction angles between 20º and 80º in increments of 0.02º. Least square fitting method is used to calculate the unit cell lattice parameter from the d-spacing and (hkl) values. By applying the Scherrer's equation on XRD pattern the crystal size of the sample is obtained. Field Effect Scanning Electron Microscopy (FE-SEM) images are taken using Carl Zeiss, EVOMA 15, Oxford Instruments, and Inca Penta FETx3.JPG is used to derive the particle morphology of the powders. Fourier transform infrared (FT-IR) spectra are obtained using Shimadzu FT-IR-8900 spectrometer using KBr pellet technique in the wavenumber range between 400 and 1000 $cm^{-1}$. Raman spectrum is recorded using Raman spectrometer (WITEC, JAPAN). An alpha 300 Raman set up equipped with 532 nm line is used to illuminate the samples at 10 mw power. VSM (Lakeshore 7300 USA) results were used to study the magnetic characteristics of the sample with an external field of 10 kOe.

## 3. RESULTS AND DISCUSSION

### 3.1 X-ray Diffraction (XRD) studies

Fig. 1 shows the XRD pattern of $SrFe_{12}O_{19}$ hexaferrites for temperature 1200 °C for 2h. The main characteristic peaks fairly collaborated with the standard diffraction pattern of $SrFe_{12}O_{19}$ (JCPDS# 80-1197) showing a single magneto-plumbite M-type hexagonal phase. However, some peaks of α-$Fe_2O_3$ (JCPDS# 80-2377) appeared as a secondary phase. It shows the peak formation and broadening after calcinations of the sample, which confirm the nano size formation of the crystals of the sample [26]. The crystallite size of the sample is calculated using the Scherrer equation, which is shown in Table 1. It shows some variation due to existence of impurity [27]. The most intense peaks (114) and (107) representing that the nonmagnetic phase increases at the expense of magneto-plumbite phase [28]. From the structural analysis, it can be confirmed that for complete crystallization, the $SrFe_{12}O_{19}$ system needs high temperatures [29].

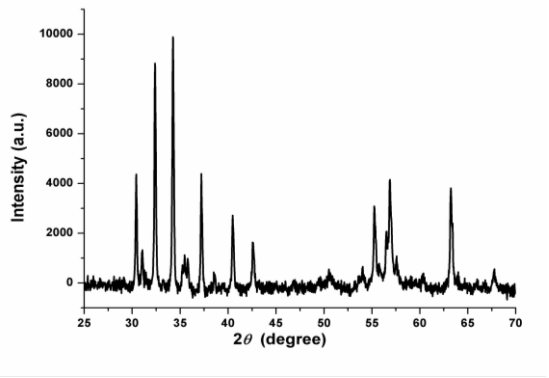


**Fig. 1**: XRD patterns for $SrFe_{12}O_{19}$ hexaferrites

**Table 1:** Lattice parameter or Cell parameter (A), Unit cell volume ($A^3$), Crystallite size (nm) of $SrFe_{12}O_{19}$ hexaferrites.

| | |
|---|---|
| Cell parameter (Å) | a = b = 5.8682<br>c = 23.09394 |
| Unit cell volume $(Å)^3$ | 688.1292 |
| Crystallite size (nm) | 59.52 |

### 3.2 Field Emission Scanning Electron Microscopy (FESEM) studies

Fig. 2 shows the micro-structural morphology and grain distribution of $SrFe_{12}O_{19}$ hexaferrites as characterized by FESEM. It is observed that most of the grains are hexagonal having sharp grain boundaries and closely packed throughout the view of the sample. It is concluded that the size and thickness of hexagonal particles leads to the growth of the particle with the formation of some agglomerates [30-31]. The primary particles which are of 1.5 µm, have typical hexa-ferrite morphology. Evidently, annealing time showed a strong effect on the morphology and size of the grains. The annealing time of 2 h is optimized [32]. This further shows that the applied sol-gel auto-combustion method for synthesis of hexaferrites material is an effective method. The elemental composition of the constituents as elicited from EDS (fig. 3), shows that the initial stoichiometric ratio of synthesized material.

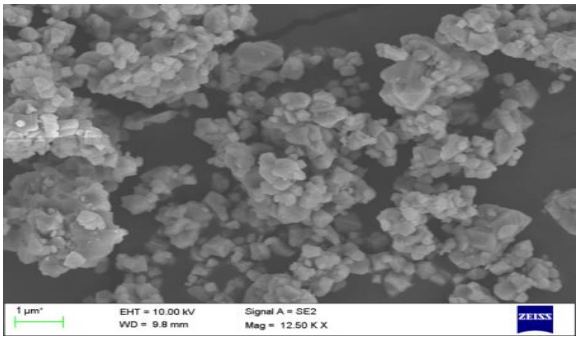


**Fig. 2: FE**-SEM micrograph of $SrFe_{12}O_{19}$ hexaferrites

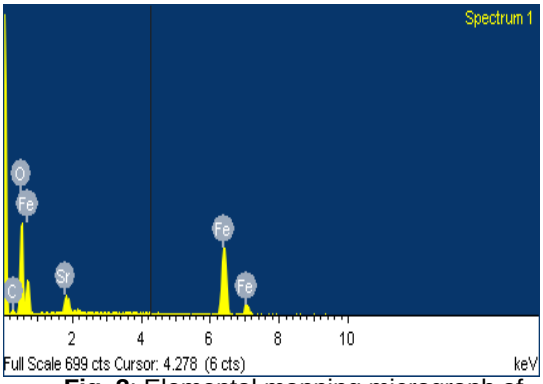


**Fig. 3**: Elemental mapping micrograph of $SrFe_{12}O_{19}$ hexaferrites

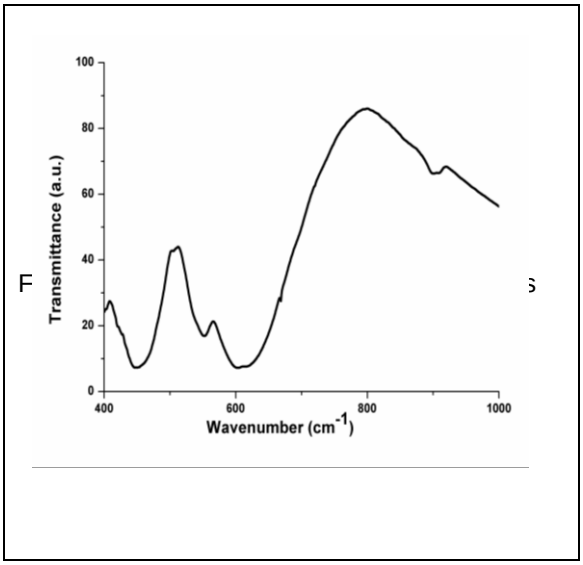


F s

### 3.3 Fourier Transform Infrared Spectroscopy (FT-IR) Studies

The FT-IR spectrum of $SrFe_{12}O_{19}$ hexaferrites is recorded at room temperature. The wave number range is taken from 400 to 1000 $cm^{-1}$ as shown in fig. 4. The frequency bands in the range 430-475 $cm^{-1}$ correspond to the characteristic peaks of lattice vibration of metal ions at octahedral sites. And the frequency bands in the range of 550-585 $cm^{-1}$ correspond to the characteristic peaks of lattice vibration of metal ions at tetrahedral sites [33]. The sharp peaks at 412 $cm^{-1}$ and 502 $cm^{-1}$ are in consistent with the characteristic peaks of stretching vibrations of metal-oxygen (M-O) bond, which indicates the formation of hexa-ferrites materials [34-35].

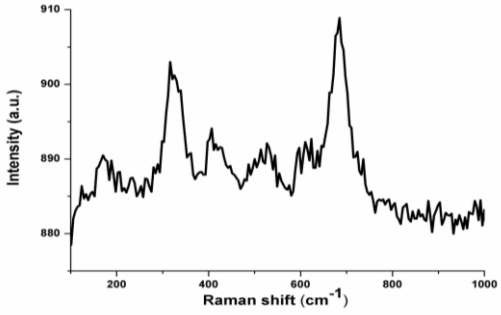


**Fig. 4:** Raman spectra of $SrFe_{12}O_{19}$ hexaferrites

### 3.4 Raman spectroscopy studies

The Raman spectra of $SrFe_{12}O_{19}$ hexaferrites material is recorded in the region of 100 to 1000 $cm^{-1}$ measured at room temperature as shown in Fig. 5. The Raman spectrum reveals that, the structure transition, lattice distortion, natural frequency, local cation distribution, spin-lattice couplings, magnetic ordering and charge-lattice. The broadening of the peak are related to the chemical composition, atomic radii, valence, bond length, cell size, and the magnetic order of the crystal of the sample [36]. According to group theory consequence, the hexagonal cell of $SrFe_{12}O_{19}$ shows $D^4_{6h}$ symmetry. These peaks belong to the localized vibrations, which are used for rapid detection and identifying of the phase. $A_{1g}$ mode has the significance of an octahedral dominated mode. The peaks, noticed at 723 $cm^{-1}$ and 688 $cm^{-1}$, are allocated to $A_{1g}$ vibrations of Fe–O bonds at the tetrahedral $4f_1$ and bi-pyramidal 2b sites. The other characteristic peaks observed at 616 $cm^{-1}$, 578 $cm^{-1}$, 471 $cm^{-1}$ and 301 $cm^{-1}$ are due to $A_{1g}$ vibrations of Fe–O bonds at the octahedral $4f_2$, 2a, and 12k sites. The peak noticed at 409 $cm^{-1}$ is due to $A_{1g}$ vibration at the octahedral 12k dominated site. The peaks observed at 536 $cm^{-1}$, 283 $cm^{-1}$, and 206 $cm^{-1}$ are due to $E_{1g}$ vibrations, while the peak observed at 333 $cm^{-1}$ is due to $E_{2g}$ vibration. The peaks seen at 191 $cm^{-1}$ and 179 $cm^{-1}$ result from $E_{1g}$ vibrations of the whole spinel block [37]. It is observed that the higher energy $A_{1g}$ modes in such similar spinel structures are known to be nearly unaffected ions involved but are strongly influenced by bonding.

### 3.5 Magnetic (VSM) properties

The hysteresis loops of $SrFe_{12}O_{19}$ hexaferrites are investigated by using Vibrating Sample Magnetometer at room temperature with an applied field of 10 kOe. Fig. 5 shows that, at room temperature, the $SrFe_{12}O_{19}$ displays characteristic hard magnetic property with large $H_C$ value of 1364 Oe and remanence of $M_r$ = 30.83 emu/g. The intrinsic magnetic properties of M-type hexaferrites, are strongly affected, the change in the ionic radii, density and valence state. This phenomenon is explained by means of super exchange interaction [38, 51-55]. The magnetic moment in M-type hexaferrites is due to the distribution of iron on five non- equivalent sub-lattices, in which three are octahedral (2a, 12k, and $4f_2$), one tetrahedral ($4f_1$) and one trigonal bi-pyramidal (2b) [39]. The 12k, 2a, and 2b sub-lattices have upward spins while $4f_1$ and $4f_2$ have downward spin of electrons. The total magnetic moment (20 $\mu_B$) is due to uncompensated upward spins [40].The magneton number $n_B$ ($\mu_B$) is obtained using the relation $n_B$ = (molecular weight × $M_S$)/5585, where $M_S$ is the saturation magnetization of the sample [41-42, 56-60]. The values of $M_S$, $H_C$, $M_r$ and R (= $M_r/M_S$) for $SrFe_{12}O_{19}$ are calculated from the magnetization curves as shown in Table 2.

**Table 2**: RT magnetic parameters viz .Saturation magnetization ($M_S$), Remanent magnetization ($M_r$), Coercivity ($H_C$) and Magneton number ($n_B$) of $SrFe_{12}O_{19}$ hexaferrites sample.

| Compound | $SrFe_{12}O_1$ |
|---|---|
| $M_S$(emu/g) | 58.82 |
| $M_r$(emu/g) | 30.83 |
| $M_r/M_S$ | 0.52 |
| $H_C$(Oe) | 1364 |
| $n_B(\mu_B)$ | 11.18 |

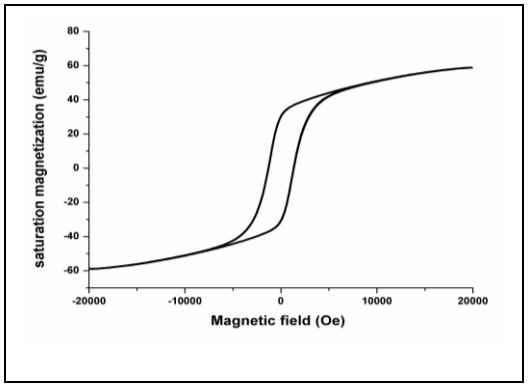


## 4 CONCLUSIONS

The sol-gel auto-combustion method is adopted to synthesize the $SrFe_{12}O_{19}$ hexaferrites sample successfully. The X-ray diffraction analysis showed that the materials have a single magneto-plumbite phase. EDS analysis confirm the nominal stoichiometry of the synthesized sample. A change in morphology of particles is observed which changed from hexagonal structure to irregular shape with the formation of some agglomerates. FT-IR spectroscopy results are in consistent with the characteristic peaks of stretching vibrations of metal - oxygen (M - O) bond which indicates the formation of hexa-ferrite. Raman spectroscopy reveals that the higher energy $A_{1g}$ modes are nearly unaffected by the metal ions involved but are strongly influenced by bonds formed. The VSM studies confirm that the strontium hexaferrites exhibit hard magnetic nature.

## 5 ACKNOWLEDGEMENTS

One of the authors A. Venkateswara Rao would like to thank the management of Koneru Lakshmaiah Education Foundation (KLEF) and Department of Science & Technology (DST-SERB), Govt. of India, for the award of DST-FIST level-I (SR/FST/PS-I/2018/35) to Department of Physics.

## REFERENCES

[1] V. F. Belov, K. S. Ovanesyan, V. A. Trukhtanov, M. N. Shwko, E.V. Korneev, V. V. Korovushkin, and L. N. Korablin., soviet physics jetp., 5, 32, (1971).
[2] J. J. Went, G.W. Ratheneau, E.W. Gorter, G.W. Van Dosterhout, Philips Tech. Rev.13 (1951).
[3] S. R. Shinde, S.E. Lofland, C.S. Ganpule, S.M. Bhagat, S.B. Bhagat, S.B. Ogale, R. Ramesh, T. Venkatesan., J. Appl.Phys.74, 594, (1999).
[4] N. Chen, K. Yang, M.Y. Gu., J. Alloys Compd.490, 609, (2010).
[5] J. Dho, E.K. Lee, J.Y. Park, N.H. Hur., J. Magn. Magn. Mater. 285, 164, (2005).
[6] Y.W. Dou, Ferrite, Jiangsu Science and Technology, Nanjing, p. 417, (1996).
[7] N. Dishovske, A. Petkov, I.V. Nedkov, IEEE Transactions on Magnetics 30, 969, (1994).
[8] C.A. Van Den Brock, A.L. Stuijts, Philips Technical Review 37, 157, (1977).
[9] O. Kubo, T. Ido, H. Yok, IEEE Transactions on Magnetics 18, 1122, (1982).
[10] Cochardt, J. Appl.Phys. 34, 1273–1274, (1963).
[11] M. Sugimoto, J. Am. Ceram. Soc. 82, 269–280, (1999).
[12] R.C. Pullar, Prog. Mater. Sci. 57, 1191–1334, (2012).
[13] V.G. Harris, A. Geiler, Y.J. Chen, S.D. Yoon, M.Z. Wu, A. Yang, Z.H. Chen, P. He, P.V. Parimi, X. Zuo, C.E. Patton, M. Abee, O. Acher, C. Vittoria., J. Magn. Magn. Mater. 321, 2035–2047, (2009).
[14] X. Tang, R.Y. Hong, W.G. Feng, D. Badami, J.Alloys Compd. 562, 211–218, (2013).
[15] Sk. Suriya Shihab, K. Govinda Rao, M. Gnana Kiran, Shaik. Babu, S. Sreehari Sastry, Rasayan J of Chemistry, 10, 1 (59 -63) 2017.
[16] K. Siva Rama Krishna Reddy, K. Swapna, Sk. Mahamuda, M. Venkateswarlu, M.V.V.K. Srinivas Prasad, A.S. Rao, G. Vijaya Prakash, 79 (2018) 21-32.
[17] Ch. B Annapurna Devi, Sk. Mahamuda, K. Swapna, M. Venkateswarlu, A. Srinivasa Rao, G. Vijaya Prakash, Optical Materials 73 (2017) 260-267.
[18] Nisha Deopa, A.S. Rao, Dr., Sk. Mahamuda, Mohini Gupta, M. Jayasimhadri, D. Haranath, G. Vijaya Prakash, Journal of Alloys and Compounds, 708 (2017) 911-921.
[19] Ch. B. Annapurna Devi, Sk. Mahamuda, M. Venkateswarlu, K. Swapna, A. Srinivasa Rao, G. Vijaya Prakash, Optical Materials 62 (2016) 569-577.
[20] M. Gnana Kirana, N. Krishna Jyothia, M. Narasimha Rao, K. Vijaya Kumar, J. Indian Chem. Soc, 96 (2019) 76-77.
[21] J. Madhuri Sailaja, N. Murali, S.J. Margarette, N. Krishna Jyothi, K. Rajkumar, V. Veeraiah, South African Journal of Chemical Engineering 26 (2018) 61–69.
[22] Talewar R.A., Mahamuda S., Swapna K., Rao A.S, Journal of Alloys and Compounds, 771 (2019) 980-986.
[23] SK.Shahenoor Basha, G.Sunita Sundari, K.Vijay Kumar, International Journal of ChemTech Research, 9, 2 (2016) 165-175.
[24] G. Sunita Sundari, K. Vijay Kumar, SK. Shahenoor Basha, M.C. Rao, Rasayan J of Chemistry, 10, 1 (298 -304) 2017.
[25] S. K. Shahenoor Basha, G. Sunita Sundari, K. Vijay Kumar, M. C. Rao, J Inorg Organomet Polym, 27, 2, (2017) 455-466.
[26] Sk. Shahenoor Basha, G. Sunita Sundari, K. Vijay Kumar, K. Ramachandra Rao, M.C. Rao, Optik, 164 (2018) 596–605.
[27] SK. Shahenoor Basha, M. Gnanakiran, B. Ranjit Kumar, K. Veera Bhadra Reddy, M.V. Basaveswara Rao, M.C. Rao, Rasayan J of Chemistry, 10, 1 (2017) 1159-1166.
[28] X. Tang, Y.M. Wang, Z. Luo, L.S. Wang, R.Y. Hong, W.G. Feng, Prog. Org. Coat. 75 124–130, (2012).
[29] T.P. Xie, L.J. Xu, C.L. Liu, Powder Technol. 232, 87–92, (2012).

[30] T.P. Xie, L. J. Xu, C. L. Liu, Y. Wang, Appl. Surf. Sci. 273, 684–691, (2013).
[31] G.M. Rai, M.A. Iqbal, K.T. Kubra, J. Alloys Compd. 495, 229, (2010).
[32] F.M.M. Pereira, C.A.R. Junior, M.R.P. Santos, R.S.T.M. Sohn, F.N.A. Freire, J.M. Sasaki, R.S.T.M. Sohn, F.N.A. Freire, J.M. Sasaki, J.A.C. de Paiva, A.S.B. Sombra., J. Mater. Sci. Mater. Electron. 19, 627, (2008).
[33] L. Lechevallier, J.M. Le Breton, A. Morel, P. Tenaud, J. Phys. Condens. Matter 20,175203, (2008).
[34] M.J. Iqbal, S. Farooq., J. Alloys Compd. 505, 560, (2010).
[35] M. Zeuner, P. J. Schmidt and W. Schnick., Chem. Mater., 21, 2467, (2009).
[36] Ataie, I.R. Harris, C.B. Ponton, J. Mater. Sci. 30, 1429–1433, (1995).
[37] M. Sivakumar, A. Gedanken, W. Zhong, Y.W. Du, D. Bhattacharya, Y. Yeshurun, I. Felner., J. Magn. Magn. Mater. 268, 95–104, (2004).
[38] J. Fang, J.Wang, L.-M. Gan, S.-C. Ng, J. Ding, X. Liu., J. Am. Ceram. Soc. 83, 1049–1055, (2000).
[39] D.H. Chen, Y.Y. Chen, J. Colloid Interface Sci. 236, 41–46, (2001).
[40] D.S. Mathew, R.S. Juang, Chem. Eng. J. 129, 51–65, (2007).
[41] Z. X. Yue, J. Zhou, L.T. Li, H.G. Zhang, Z.L. Gui., J. Magn. Magn. Mater. 208, 55–60, (2000).
[42] N Krishna Jyothi, K K Venkataratnam, P Narayana murty, K Vijaya Kumar, Bull. Mater. Sci., 39, 4, (2016) 1047–1055.
[43] J.F. Crider, Ceram. Eng. Sci. Proc. 3, 519, (1982).
[44] N. Krishna Jyothi, K. K. Venkata Ratnam, P. Narayana Murthy, K. Vijaya Kumar, Materials Today: Proceedings 3 (2016) 21-30.
[45] P. Shepherd, K.K. Mallick, R.J. Green., J. Magn. Magn. Mater. 311, 683, (2007).
[46] L.A. Garcia-Cerda, O.S. Rodriguez-Fernández, P.J. Reséndiz-Hernández., J. Alloys Compd. 369, 182–184, (2004).
[47] N Krishna Jyothi, K Vijaya Kumar, G Sunita Sundari, P Narayana Murthy, Indian J Phys (March 2016) 90(3):289–296.
[48] Q.Q. Fang, H. Cheng, K. Huang, J. Wang, R. Li, Y. Jiao., J. Magn. Magn. Mater. 294, 281, (2005).
[49] N. Rezlescu, C. Doroftei, E. Rezlescu, P.D. Popa., J. Alloys Compd. 451, 492, (2008).
[50] X. Wu, K. Zhou, W. Wu, X. Cui, Y. Li., J. Therm. Anal. Calorim. (2011).
[51] J.R. Liu, R.Y. Hong, W.G. Feng, D. Badami, Y. Q. Wang Powder Technology 262, 142-149, (2014)
[52] Raghavendra Vemuri, G. Rajub, M. Gnana Kiranc, M.S.N.A. Prasadd, E. Rajesh, G. Pavan Kumare, N. Murali, Results in Physics 12 (2019) 947–952.
[53] Ramakrishna, N. Murali, S.J. Margarette, Tulu Wegayehu Mammo, N. Krishna Joythi, B. Sailaja, Ch.C. Sailaja Kumari, K. Samatha, V. Veeraiah, Advanced Powder Technology 29 (2018) 2601–2607.
[54] S. Singhal, T. Namgyal, J. Singh, K. Chandra, S. Bansal., Ceram. Int. (2011).
[55] M.N. Ashiq, M.J. Iqbal, I.H. Gul., J. Alloys Compd. 487, 341, (2009).
[56] Ankush Thakur, R.R. Singh, P.B. Barman., J. Magn. Magn. Mater 326, 35–40, (2013).
[57] J.P. Singh, G. Dixit, R.C. Srivastava, H.M. Agrawal, K. Asokan., J. Phys. D Appl. Phys. 44, 435306, (2011).
[58] J. Kreisel, G. Lucazeau, and H. Vincent., J. Raman Spectrosc. 30 (2), 115, (1999).
[59] J. Kreisel, G. Lucazeau, and H. Vincent., J. Solid State Chem. 137, 127, (1998).
[60] W.Y. Zhao, P. Wei, X.Y. Wu, W. Wang, and Q. J. Zhang., J. Appl. Phys. 103, 063902 (2008).